A short C-terminal peptide in Gγ regulates Gβγ signaling efficacy

Mithila Tennakoon[a,†], Kanishka Senarath[a,†,‡], Dinesh Kankanamge[a,§], Deborah N. Chadee[b], and Ajith Karunarathne[a,*]

[a]Department of Chemistry and Biochemistry and [b]Department of Biological Sciences, The University of Toledo, Toledo, OH 43606

ABSTRACT G protein beta-gamma (Gβγ) subunits anchor to the plasma membrane (PM) through the carboxy-terminal (CT) prenyl group in Gγ. This interaction is crucial for the PM localization and functioning of Gβγ, allowing GPCR-G protein signaling to proceed. The diverse Gγ family has 12 members, and we have recently shown that the signaling efficacies of major Gβγ effectors are Gγ-type dependent. This dependency is due to the distinct series of membrane-interacting abilities of Gγ. However, the molecular process allowing for Gβγ subunits to exhibit a discrete and diverse range of Gγ-type–dependent membrane affinities is unclear and cannot be explained using only the type of prenylation. The present work explores the unique designs of membrane-interacting CT residues in Gγ as a major source for this Gγ-type–dependent Gβγ signaling. Despite the type of prenylation, the results show signaling efficacy at the PM, and associated cell behaviors of Gβγ are governed by crucially located specific amino acids in the five to six residue preprenylation region of Gγ. The provided molecular picture of Gγ–membrane interactions may explain how cells gain Gγ-type–dependent G protein-GPCR signaling as well as how Gβγ elicits selective signaling at various subcellular compartments.

Monitoring Editor
Peter Van Haastert
University of Groningin

Received: Nov 30, 2020
Revised: May 3, 2021
Accepted: Jun 4, 2021

INTRODUCTION

G protein heterotrimers (Gαβγ) interact with the inner leaflet of the plasma membrane (PM) primarily through their covalent lipid modifications (fatty acylations). These modifications provide an additional layer of G protein activity regulation (Wedegaertner *et al.*, 1995; Resh, 2013). G protein α (Gα) subunits are N-terminally (NT) modified with a 14-carbon (14-C) myristate and/or a 16-C palmitate group, while G protein γ (Gγ) subunits are prenylated at their carboxy-terminal (CT) (Wedegaertner *et al.*, 1995; Pedone and Hepler, 2007). Prenylation of the 12 Gγ types, with either a 20-C isoprenoid geranylgeranyl or a 15-C farnesyl group, involves stable thioether bond formation at the CaaX motif *cys* in the Gγ CT (Wedegaertner *et al.*, 1995). Despite being anchored to the PM by just one of the

This article was published online ahead of print in MBoC in Press (http://www.molbiolcell.org/cgi/doi/10.1091/mbc.E20-11-0750) on June 9, 2021.

†Equal contributions.

Conflict of interest: The authors declare that they have no conflicts of interest with the contents of this article.

Author contributions: K.S. generated all the Gγ mutants. M.T. and K.S. collectively performed all the experiments. D.K. assisted in PIP2-hydrolysis experiments. M.T. analyzed the data and prepared the figures. D.N.C provided reagents and experimental support. M.T., K.S., and A.K. conceptualized the project and wrote the manuscript.

Present addresses: ‡Institute of Biochemistry, Molecular Biology and Biotechnology, University of Colombo, Colombo 00300, Sri Lanka; §Department of Anesthesiology, Washington University School of Medicine, St. Louis, MO 63110.

*Address correspondence to: Ajith Karunarathne (ajith.karunarathne@utoledo.edu).

Abbreviations used: AFU, arbitrary fluorescence units; ANOVA, Analysis of Variance; ATCC, American Type Culture Collection; CT, carboxy terminus; DAG, diacylglycerol; DFBS, dialyzed fetal bovine serum; DNA, deoxyribonucleic acid; EDTA, ethylenediaminetetraacetic; EMCCD, electron multiplying charge-coupled device; ER, endoplasmic reticulum; FRAP-PA, fluorescence recovery after photobleaching and photoactivation; FRET, förster resonance energy transfer; GDP, guanosine diphosphate; GFP, green fluorescence protein; GIRK, G protein-coupled inwardly-rectifying potassium channels; GPCR, G protein-coupled receptor; GRK2, G protein-coupled receptor kinase 2; GRPR, gastrin-releasing peptide receptor; GTP, guanosine triphosphate; HBSS, Hanks' balanced salt solution; ICMT, Isoprenylcysteine Carboxyl Methyltransferase; IM, internal membrane; IP3, inositol trisphosphate; mCh, mCherry; MEM, minimum essential medium; NEI, national eye institute; NLFit, nonlinear curve fitting; NT, amino terminus; PCR, polymerase chain reaction; PH, pleckstrin homology; PI3K, phosphoinositide 3-kinase; PIP2, phosphatidylinositol (4,5)-bisphosphate; PIP3, phosphatidylinositol (3,4,5)-trisphosphate; PLCβ, phospholipase C β; PM, plasma membrane; PS, Penicillin–Streptomycin; RCE1, Ras Converting CAAX Endopeptidase 1; ROI, region of interest; SD, standard deviation; SEM, standard error of mean; STR, short tandem repeat; TIRF, total internal reflection fluorescence; WT, wild type.

two possible prenyl attachments, Gβγ shows multiple Gγ-type–dependent PM affinities and signaling abilities (O'Neill *et al.*, 2012; Senarath *et al.*, 2018). For instance, the expression of Gγ3, which exhibited the highest PM affinity, allowed cells to achieve the highest Gβγ-effector activation at the PM (O'Neill *et al.*, 2012; Senarath *et al.*, 2018). On the contrary, cells expressing Gγ9, the Gγ with the lowest PM affinity, showed almost no Gβγ-effector activation. In these studies, we measured the PM affinity by taking the inverse half-time of Gβγ translocation from the PM to internal membranes (IMs) induced by GPCR activation.

Besides prenyl anchor–PM interactions, interactions between residues in the CT of Gγ with the PM have also been shown (Matsuda *et al.*, 1994; Higgins and Casey, 1996). The PM possesses a phospholipid bilayer structure with embedded proteins and forms a fluidic mosaic (Singer and Nicolson, 1972; Engelman, 2005). The major phospholipid constituents of the PM are phosphatidylethanolamine, phosphatidylserine, phosphatidylinositol, phosphatidylcholine, and sphingomyelin (Hessel *et al.*, 2003; Jastrzebska *et al.*, 2011; Khan *et al.*, 2013). These lipids contain two acyl lipid anchors linked to a polar phosphate head group via a glycerol molecule. Their negatively charged hydrophilic head groups face the cytosol, while the acyl groups form the core of the PM bilayer. Because the polar head groups of both phosphatidylserine and phosphatidylinositol are negatively charged, their predominance provides a net negative charge to the inner leaflet of the PM (Dowhan, 1997; Knight and Falke, 2009). Changes in the PM lipid composition have been shown to alter its association with G proteins (Escriba *et al.*, 2003; Vogler *et al.*, 2004).

We have demonstrated that Gγ3 and Gγ2 possess the highest PM affinity and their expression provides cells with the highest Gβγ-effector activities at the PM (Senarath *et al.*, 2018). Both Gγ2 and Gγ3 possess hydrophobic *phe* and positively charged *lys* and *arg* residues at their preprenylation (pre-CaaX) region. However, the pre-CaaX regions of Gγ with low PM affinity and low effector activation ability (i.e., Gγ*9*, Gγ1) contain neutral *gly* and negatively charged *glu* residues (O'Neill *et al.*, 2012; Senarath *et al.*, 2018). Therefore, we hypothesize that the Gγ-dependent differential effector activation abilities of Gβγ at the PM are governed by the CT residues of Gγ subtypes as well as the chemical properties of the PM. Additionally, the three-dimensional structure of a protein is crucial for its biological functions and is determined by both its primary sequence and the surrounding chemical environment (Anfinsen, 1973; Das *et al.*, 2015). PM-interacting proteins are either embedded in or interacting with the PM, and their structure-function attributes are heavily influenced by the properties of the PM. The fluid mosaic membrane structure permits several modes of movement to the proteins interacting with the bilayer. Rotational movements allow proteins to sample their immediate neighborhood and interact with effectors (Simons and Vaz, 2004; Engelman, 2005). Lateral diffusion enables proteins to migrate from one PM microdomain to another and reach distant effector molecules (Hepler, 2014; Czysz *et al.*, 2015). Lateral mobilities of proteins in biological membranes are affected by the degree of crowding, membrane domains (i.e., lipid rafts), and interactions with cytoskeletal components (Frick *et al.*, 2007; Owen *et al.*, 2009; Ramadurai *et al.*, 2010). The crystal structure of GRK2-Gβγ shows a rotation of Gβγ by ~90°, while moving more than 100 Å from the origin, which 1) allows for Gβγ-GRK2 interaction to take place and 2) exposes both the receptor and GαqGTP to GRK2 (Tesmer *et al.*, 2005; Nishimura *et al.*, 2010; Samaradivakara *et al.*, 2018). Therefore, lateral and rotational movements of Gβγ on the PM are likely to affect the activation of other Gβγ effectors as well. Because several CT residues of Gγ interact with the PM, we propose that differential sequence properties of CT domains in Gγ subtypes result in distinct lateral as well as rotational movements of Gβγ at the PM, regulating the efficacy of the associated Gβγ signaling.

Like Gγ, many other G proteins, including Ras and Ras-like proteins, comprise a pre-CaaX and a prenylated-*cys,* encoded by the CaaX motifs at their CT (Seabra, 1998; Maurer-Stroh *et al.*, 2007). These proteins play critical roles in many cellular functions, including regulation of protein trafficking, cell proliferation, differentiation, and survival (Seabra, 1998; Wennerberg *et al.*, 2005; Vogler *et al.*, 2008). However, compared with the severalfold-longer and primarily polybasic pre-CaaX regions in Ras proteins, the five to six residue short pre-CaaX in Gγ is unique. Further, among Gγ subtypes, only Gγ2, γ3, and γ4 possess a distinctive hydrophobic character in the pre-CaaX. Therefore, we ask what functional roles pre-CaaX residues in Gγ play in tuning Gβγ signaling.

RESULTS

Selection criteria of residues in Gγ-CT to tune Gβγ–PM interactions

Besides prenylation, Ras superfamily proteins use a 15–20 residue polybasic pre-CaaX region for PM anchoring, establishing electrostatic interactions with the PM. To understand how Gγ accomplishes sufficient PM anchoring by using only a five to six residue pre-CaaX region, we examined the chemistry of its individual residues. All Gγ types (except Gγ13) possess a conserved *phe* residue, that is, *phe*65 in Gγ3 and *phe*60 in Gγ*9*, which functions as the last Gβ contact point (Figure 1A, blue box). The pre-CaaX region spans from this conserved *phe* to prenylated-*cys*. Owing to its proximity, this region is likely to interact with the PM (Figure 1B). Among the 12 Gγ subtypes, Gγ*9* imparts the highest GPCR activation-induced translocation rate (from the PM to IMs) for Gβγ (O'Neill *et al.*, 2012; Senarath *et al.*, 2018). Therefore, Gγ*9* expression allows cells to maintain the lowest Gβγ concentration, as well as the lowermost Gβγ-effector signaling at the PM (O'Neill *et al.*, 2012; Senarath *et al.*, 2018). Contrarily, Gγ3 exerts the lowest translocation rate for Gβγ, and thus cells could maintain the highest Gβγ-effector activity at the PM. In addition to the type of prenylation, we have previously shown evidence for pre-CaaX region-regulated control of the PM affinity and effector activity of Gβγ at the PM (Ajith Karunarathne *et al.*, 2012; Senarath *et al.*, 2018). Pre-CaaX sequences such as those in Gγ3 contain primarily positively charged and hydrophobic amino acids (Figure 1A, underlined). Thus, we postulate that the positively charged amino acids establish electrostatic interactions with the negatively charged phospholipid head groups. The hydrophobic residues interact with the hydrophobic core of the PM (Figure 1C, top) (Senarath *et al.*, 2018).

Therefore, to examine how Gγ types yield a discrete series of PM affinities for Gβγ, regulating its signaling at the PM using one of the two possible lipid anchors, we systematically mutated pre-CaaX residues (Figure 1A, green box) in both Gγ3 and Gγ*9*. Because these Gγ types provide the two extreme PM affinity characteristics for Gβγ, our strategy was to generate Gγ3-like mutants from farnesylated Gγ*9* and Gγ*9*-like mutants from geranylgeranylated Gγ3, by altering only residues in their pre-CaaX regions. We have previously demonstrated that the transfected Gγ type becomes the most prominent and the dominant Gγ over the endogenous Gγs in a cell line (Senarath *et al.*, 2018). This observation agrees with Gγ-specific distinct signaling changes observed in cells upon Gγ transfection. While the expression-level differences of Gγ among cells can influence the extent of their effects, we mitigate this by considering cells with only a defined green fluorescent protein (GFP)-Gγ–expression

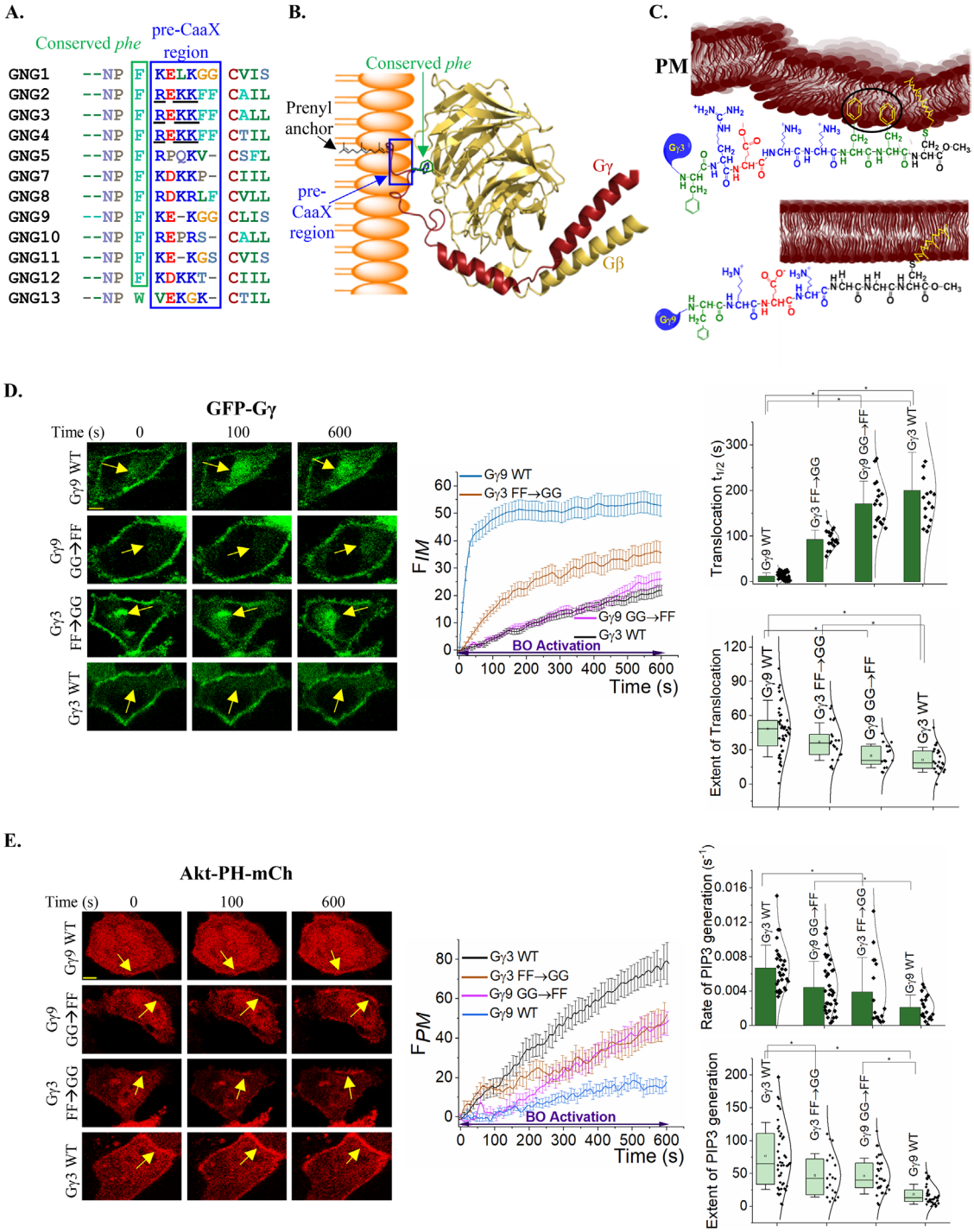

FIGURE 1: Molecular rationale for Gβγ PM-affinity control by preprenylation (pre-CaaX) residues of Gγ and the importance of *phe-duo* next to the prenylated-*cys* in Gγ3 to enhance Gβγ PM-affinity and PI3K activation. (A) Sequence alignment of the CT regions of the 12 Gγ subtypes. Conserved *phe*: green box, pre-CaaX region: blue box, and prenylated *cys*: brown, which undergoes prenylation and carboxymethylation. (B) Gβγ crystal structure (PDB ID: 2BCJ) modified to show its interaction with the PM using PyMOL software. The blue box: pre-CaaX, green residue: the conserved *phe* (the last GγG–β contact). The prenyl anchor–PM interaction is shown in black. (C) Hypothesized interactions between the CT of Gγ*9* and Gγ3 with the PM. Polar-charged and hydrophobic groups in pre-CaaX residues interact with polar head groups and the hydrophobic core of the PM, respectively. Negatively charged *glu* (red) residues likely to modulate Gγ–PM interactions. This model provides molecular reasoning for PM-affinity differences among Gγ members including Gγ*9* and Gγ3. Chemical structures were drawn using ChemDraw software. (D) Time-lapse images of HeLa cells expressing GFP-Gγ*9*, Gγ3, or their mutants with the Gi/o-coupled light-sensing GPCR, blue opsin before and after GPCR activation. Cells incubated with 10 μM 11-*cis*-retinal upon exposure to blue light show Gγ-type–dependent Gβγ translocation from the PM to IMs. Yellow arrows indicate the IMs. The plot shows Gγ translocation measured using F_{IM} (IM fluorescence). Scale bar: 5 μm. Average curves were plotted using $n \geq 10$ cells from ≥3 independent

range for translocation and signaling measurements. For instance, we use a constant excitation intensity and consider only cells with an approximately ±30% emission range. This range is selected because these cells show a predominantly PM-bound Gγ with a minor presence at the IMs (Thul *et al.*, 2017). As shown in sample images in Figure 1D, the selection of cells with a defined range of fluorescence intensities allows us to have cells with near-similar Gγ WT and mutant expressions for signaling quantification.

Two phe residues (phe-duo) adjacent to the prenylated-cys in Gγ3 are essential for the enhanced PM affinity and PI3K activation of Gβγ. Gγ sequences display two distinct groups of residues in their pre-CaaX region: nonhydrophobic as in Gγ1, γ5, γ7, γ9, γ10, γ11, γ12, and γ13 and hydrophobic as in Gγ2, γ3, γ4, and γ8. Gγ3, γ2, and γ4 provide the highest Gβγ-governed PI3K (phosphatidylinositol 3-kinases) activation (Senarath *et al.*, 2018). All of them possess a conserved *phe-duo* next to the prenylated and carboxymethylated *cys*. Therefore, we predicted that benzyl groups in *phe* residues interact with the PM, strengthening Gγ anchoring to the PM (Figure 1C, top, black circle). In contrast, Gγ9 possesses two *gly* residues next to the prenylated-*cys* and is expected to interact with the PM relatively loosely (Figure 1C, bottom). To explore these hypotheses, we systematically mutated pre-CaaX residues in Gγ3 and Gγ9. To gain the precise temporal control of GPCR-G protein activation using optogenetic signaling control, we expressed the light-sensitive Gi/o-coupled GPCR, blue opsin, and examined the behaviors of mutant Gγs compared with their WTs upon GPCR activation. Cells were incubated with 11-*cis*-retinal to make blue opsin light-activatable. GPCR activation-induced translocation of Gγ (and their mutants) was imaged using amino terminally (NT) GFP-tagged Gγ. Blue opsin was activated by exposing cells to 445 nm blue light at 1 Hz.

When the *phe-duo* in Gγ3 was replaced with two *gly* residues (Gγ3-*phe-phe→gly-gly*: NPFREKKGGCALL) compared with the WT Gγ3 ($t_{1/2}$ = 200 ± 20 s), the mutant-expressing cells exhibited more than twofold faster translocation ($t_{1/2}$ = 93 ± 5 s) (Figure 1D, images, plot, bar graph, and Table 1) (one-way analysis of variance [ANOVA]: $F_{1, 44} = 14.98$, $p = 3.55 \times 10^{-4}$; Supplemental Table S1, A and B). In addition, this Gγ3-*phe-phe→gly-gly* mutant showed a significantly higher extent of Gβγ translocation (~76%) over that of WT Gγ3 (Figure 1D, plot, box plot, and Table 1) (one-way ANOVA: $F_{1, 44} = 14.98$, $p = 3.54 \times 10^{-4}$; Supplemental Table S2, A and B). This Gγ3 mutant is still expected to be geranylgeranylated because it carries the residues *CALL* as the CaaX motif, similar to WT Gγ3 (Wedegaertner *et al.*, 1995). The ability of translocation as Gβγ upon GPCR activation, and its predominant PM-bound cellular distribution, indicate that the Gγ3-*phe-phe→gly-gly* mutant is functional in the Gβγ heterotrimer. Therefore, the observed significant changes in Gβγ translocation in these mutant-expressing cells indicate that, in addition to the type of prenylation, the *phe-duo* in the pre-CaaX is also crucial for Gβγ–PM interactions. Because WT Gγ3 cells exhibit a robust PIP3 production upon Gi/o-coupled GPCR activation (Senarath *et al.*, 2018), we examined PIP3 production in Gγ3-*phe-phe→gly-gly* (NPFREKKGGCALL) mutant-expressing HeLa cells. Compared with WT Gγ3 cells, the extent of PIP3 generation in mutant Gγ3 cells was significantly reduced (by ~38%) (one-way ANOVA: $F_{1, 65} = 5.73$, p = 0.02). A Tukey post hoc test showed that the mean extent of PIP3 generation in mutant Gγ3 cells (47.1 ± 7.3 arbitrary fluorescence units [AFU]) is significantly lower than that in WT Gγ3 cells (76.6 ± 7.4 AFU) (Figure 1E, plot and box plot; Supplemental Table S2, A and B). Additionally, mutant Gγ3 cells showed a significantly attenuated rate of PIP3 generation (3.9×10^{-3} s^{-1}) compared with WT Gγ3 cells (6.7×10^{-3} s^{-1}) (Figure 1E, images, plot, bar graph, and Table 2) (one-way ANOVA: $F_{1, 43} = 7.67$, p = 0.0083; Supplemental Table S3, A and B).

To further validate the crucial role of this *phe-duo* in regulating the PM affinity, and the efficacy of Gβγ-mediated PI3K activation, we replaced the two adjacent *gly* residues next to prenylated-*cys* in Gγ9 with two *phe* residues (Gγ9-*gly-gly→phe-phe*: NPFKEKFFCLIS). Compared with WT Gγ9 cells (12 ± 1 s), these mutant Gγ9 cells (171 ± 12 s) exhibited an ~14-fold higher $t_{1/2}$, indicating a slower Gβγ translocation (Figure 1D, images, plot, bar graph, and Table 1) (one-way ANOVA: $F_{1, 60} = 431.24$, $p = 4.41 \times 10^{-29}$; Supplemental Table S1, A and B). Compared with WT Gγ9 cells, this mutant also exhibited a significant reduction (~50%) in the translocation extent (Figure 1D, images, plot, box plot, and Table 1) (one-way ANOVA: $F_{1, 59} = 13.62$, $p = 4.90 \times 10^{-4}$; Supplemental Table S2, A and B). Although Gγ9 expression suppresses Gβγ-induced PIP3 production in HeLa cells (rate = 2.1×10^{-3} s^{-1}), Gγ9-*gly-gly→phe-phe* mutant cells exhibited a significantly enhanced rate of PIP3 production (4.5×10^{-3} s^{-1}) (one-way ANOVA: $F_{1, 66} = 28.58$, $p = 1.20 \times 10^{-6}$). A Tukey post hoc test showed that the mean extent of PIP3 generation in Gγ9 mutant-expressing cells (46.2 ± 4.9 AFU) is more than twofold higher than that in WT-Gγ9–expressing cells (18.2 ± 2.5 AFU) (Figure 1E, images, plot, box plot, and Table 1) (Supplemental Table S4, A and B). Overall, these data suggest that *phe-duo* next to the prenylated-*cys* in Gγ significantly enhances the PM affinity and PI3K signaling of Gβγ. Additionally, compared with Gγ3 WT, Gγ3-*phe-phe→gly-gly* mutant heterotrimers showed a clear IM presence (Figure 1D, bottom images, yellow arrows). Further, Gγ9-*gly-gly→phe-phe* mutant heterotrimers exhibited a more prominent PM-bound distribution than Gγ9 WT (Figure 1D, bottom images). Therefore, these data indicate that the relative changes to Gγ PM affinity due to the presence of the *phe-duo* or lack thereof also controls heterotrimer-PM interactions. We next examined the förster resonance energy transfer (FRET) between GFP-Gγ and mCh-Gβ1 to examine intact Gβγ dimer formation. Similar to their WT Gγs, both Gγ3 and Gγ9 mutants exhibited comparable FRET changes (donor/FRET ratios) upon photobleaching the acceptor (mCh) (Supplemental Figure S1). This indicates that the above pre-CaaX mutations in Gγ do not disrupt Gγ-Gβ interactions.

Because we explore the unique designs of membrane-interacting Gγ pre-CaaX residues as a major source for Gγ-type–dependent Gβγ signaling, we specifically selected Gγ3 and Gγ9 because they respectively represent a geranylgeranylated and a farnesylated Gγ,

experiments. Error bars: SEM. The bar graph and the whisker box plot show the half-time ($t_{1/2}$) and the extents of translocation, respectively. Note the Gγ3-like properties in the Gγ9-mutant and Gγ9-like behavior in the Gγ-3 mutant. Error bars: SD. (E) Time-lapse images of HeLa cells expressing GFP-Gγ9, Gγ3, or their mutants, with blue opsin and the PIP3 sensor (Akt-PH-mCh). Cells show Gγ-type–dependent PIP3 generation at the PM upon blue opsin activation. Yellow arrows indicate the Akt-PH-mCh accumulation at the PM. The corresponding plot shows the dynamics of PIP3 generation in cells with different Gγ types, measured using the mCh fluorescence at the PM (F_{PM}). Scale bar: 5 μm. Average curves plotted using $n \geq 10$ cells from ≥3 independent experiments. Error bars: SEM. Bar graph shows distinct rates of PIP3 generation, and the whisker box plot shows the variation in the extent of PIP3 generation exhibited by WT Gγs and their mutants. Error bars: SD; *$p < 0.05$.

Gγ type	Sequence	$t_{1/2}$ (s)	Extent of translocation (AFU)
Gγ3 WT	NPFREKKFFCALL	200 ± 20	21.3 ± 2.2
Gγ3-FF→GG	NPFREKKGGCALL	93 ± 5	37.1 ± 3.6
Gγ3-FF shifted	NPFFFREKKCALL	56 ± 5	40.76 ± 3.17
Gγ3-KK→GG in FF shifted	NPFFFREGGCALL	29 ± 3	51.7 ± 14.7
Gγ3-F65→G	NPGREKKFFCALL	115 ± 18	29.7 ± 3.7
Gγ3-RE→GGGG	NPFGGGGKKFFCALL	134 ± 6	22.3 ± 11.9
Gγ9 WT	NPFKEKGGCLIS	12 ± 1	48.4 ± 3.7
Gγ9-GG→FF	NPFKEKFFCLIS	171 ± 12	24.7 ± 2.6
Gγ9-KEK→GGG	NPFGGGGGCLIS	13 ± 2	30.1 ± 8.5
Gγ9 with Gγ3 pre-CaaX	NPFREKKFFCLIS	110 ± 5	13.6 ± 4.0

AFU: Arbitrary fluorescence units.

TABLE 1: Translocation properties of Gγ mutants.

as well as demarcate the two extreme ends of the Gγ-PM–affinity range. The aim was to generate mutants with moderate-PM affinities. When we examined tissue-specific expression, Gγ types such as Gγ5, 10, and 12 show dominant expressions in most tissues (Tennakoon *et al.*, 2021). Though these Gγs are geranylgeranylated, they occupy the moderate-PM–affinity range. The primary difference between the above Gγs and Gγ3 is that they do not possess the *phe-duo* in the pre-CaaX. When we mutated Gγ3-WT to Gγ3-*phe-phe→gly-gly*, the mutant exhibited translocation properties more similar to those of Gγ5, 10, and 12 than to those of Gγ3. The translocation $t_{1/2}$ in Gγ3-WT (200 s) was changed to 93 s in the Gγ3-*phe-phe→gly-gly* mutant, similar to 70–100 s $t_{1/2}$ in moderate-PM-affinity Gγs. On the contrary, the *gly-gly→phe-phe* mutation in Gγ9 changed the $t_{1/2}$ from 12 s to 171 s. Our newly added data show that this Gγ9-*gly-gly→phe-phe* mutant remains farnesylated (Supplemental Figure S2), while the Gγ3-*phe-phe→gly-gly* mutant is geranylgeranylated. The use of Gγ3, Gγ9, and their mutants, therefore, allowed us to demonstrate the significant role of pre-CaaX in modulating the PM affinity of Gβγ using a limited number of mutations.

Location of the phe-duo in the Gγ3 pre-CaaX motif is crucial for the PM affinity of Gβγ. The above Gγ3 and Gγ9 mutants (Figure 1, D and E, and Table 1) established that the *phe-duo* significantly enhances the PM affinity and signaling activation ability of Gβγ at the PM. Among all prenylated G proteins, including heterotrimeric and Ras family members, only Gγ3, γ2, and γ4 possess this unique *phe-duo* next to the prenylated-*cys* (Supplemental Figure S3). Interestingly, cells expressing these Gγ types showed robust PI3K and PLCβ activations upon Gi pathway activation (Senarath *et al.*, 2018). Therefore, to examine whether the location of *phe-duo* in the pre-CaaX region of Gγ tunes the PM-anchoring strength of Gβγ, a Gγ3 mutant was generated by shifting *phe-duo* to the beginning of the pre-CaaX region (Gγ3-*phe-phe* shifted: NPFFFREKKCALL). Compared with WT-Gγ3 HeLa cells ($t_{1/2}$ = 200 ± 20 s), mutant Gγ3 cells ($t_{1/2}$ = 56 ± 5 s) exhibited a nearly fourfold decrease in the translocation $t_{1/2}$ upon blue opsin activation (Figure 2A and Table 1). This indicates faster Gβγ translocation in mutant Gγ3-expressing cells. Additionally, a one-way ANOVA ($F_{1, 38} = 27.01$, $p = 7.16 \times 10^{-6}$) and Tukey post hoc tests showed an approximately twofold increase in the extent of translocation for mutant Gγ3 compared with the WT-Gγ3 (40.8 ± 3.2 vs. 21.3 ± 2.2 AFU). Cells expressing this mutant also exhibited a significant reduction in the rate of PIP3 generation (4.4×10^{-3} s^{-1}) compared with WT-Gγ3 cells (6.7×10^{-3} s^{-1}) (Figure 2B and Table 2). A one-way ANOVA ($F_{1, 53} = 8.54$, $p = 0.005$) determined that there is a significant reduction in PIP3 generation in Gγ3-*phe-phe*–shifted mutant cells compared with that of WT-Gγ3 cells (56.6 ± 8.5 vs. 76.6 ± 7.4 AFU).

To examine whether the observed activity in the Gγ3-*phe-phe*–shifted mutant is due to the polybasicity of the pre-CaaX region, we

Gγ type	Sequence	Rate of PIP3 generation (10^{-3} s^{-1})	Extent of PIP3 generation (AFU)
Gγ3 WT	NPFREKKFFCALL	6.7 ± 0.3	76.6 ± 7.4
Gγ3-FF→GG	NPFREKKGGCALL	4.0 ± 0.1	47.1 ± 7.3
Gγ3-FF shifted	NPFFFREKKCALL	4.4 ± 0.6	56.6 ± 8.5
Gγ3-KK→GG in FF shifted	NPFFFREGGCALL	4.2 ± 0.6	68.4 ± 6.4
Gγ3-F65→G	NPGREKKFFCALL	4.0 ± 0.4	54.9 ± 6.2
Gγ3-RE→GGGG	NPFGGGGKKFFCALL	5.1 ± 0.2	51.3 ± 7.1
Gγ9 WT	NPFKEKGGCLIS	2.1 ± 0.3	18.3 ± 2.5
Gγ9-GG→FF	NPFKEKFFCLIS	4.5 ± 0.5	46.2 ± 4.9
Gγ9-KEK→GGG	NPFGGGGGCLIS	2.7 ± 0.4	33.9 ± 5.5
Gγ9 with Gγ3 pre-CaaX	NPFREKKFFCLIS	4.0 ± 0.7	49.1 ± 3.8

TABLE 2: PIP3 generation properties of Gγ mutants.

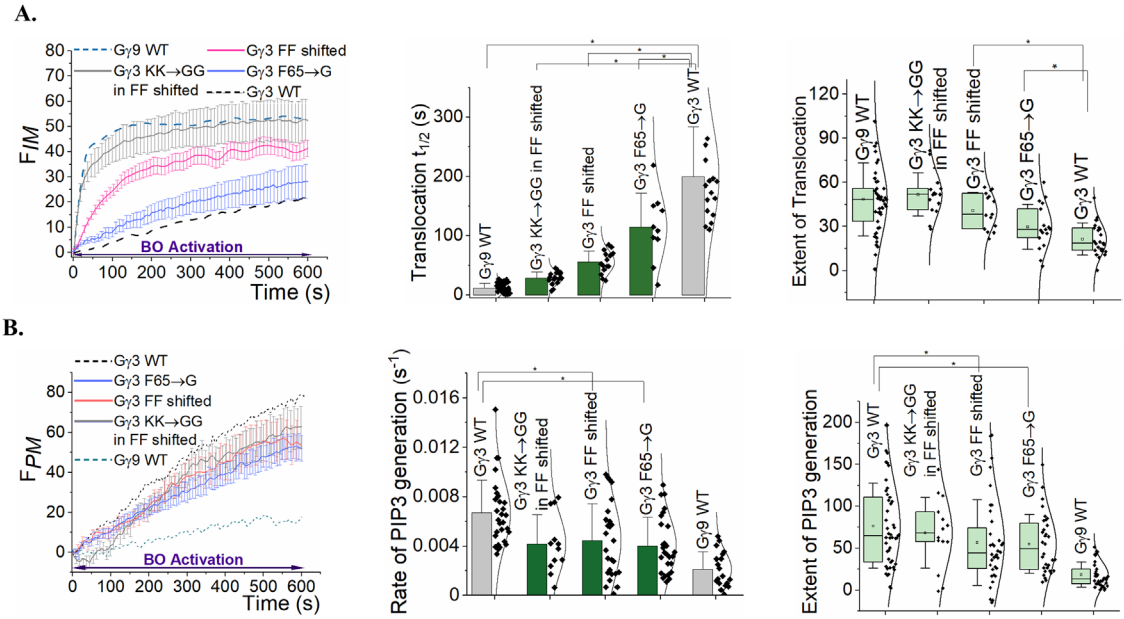

FIGURE 2: Tuning of PM affinity and PI3K activation ability of Gβγ by the relative location of *phe-duo* in pre-CaaX and the last Gβ-interacting *phe* in Gγ. (A) The plot shows the variation in the kinetics of Gβγ translocation from the PM to IMs in HeLa cells expressing Gγ3 mutants compared with WT-Gγ3 and Gγ9–expressing cells, with blue opsin activation upon exposure to blue light after incubating cells with 10 μM 11-*cis*-retinal (F_{IM} ,IM fluorescence). Average curves plotted using $n \geq 10$ cells from ≥ 3 independent experiments. Error bars: SEM. Bar graph shows the differences in translocation $t_{1/2}$ values while whisker box plot shows the variation in translocation extents in WT and mutant Gγ-expressing cells. Error bars: SD. (B) The plot shows the variance in the PIP3 generation kinetics in Gγ3 mutant–expressing cells compared with WT-Gγ3 and Gγ9–expressing cells upon blue opsin activation (F_{PM}, PM fluorescence). Average curves plotted using $n \geq 10$ cells from ≥3 independent experiments. Error bars: SEM. Bar graph shows different rates of PIP3 generation while the whisker box plot compares the magnitudes of PIP3 generation. Error bars: SD; *$p < 0.05$.

mutated the two *lys* residues located just before the CaaX motif in the Gγ3-*phe-phe*–shifted mutant (NPFFFREKKCALL) to two *gly* residues (Gγ3-*lys-lys*→*gly-gly*: NPFFFREGGCALL). Gγ3-NPFFFREGGCALL mutant cells exhibited only a minor increase in Gβγ translocation as indicated by its slightly reduced $t_{1/2}$ (29 ± 3 s) with a statistically similar translocation extent (at $p = 0.05$) compared with the Gγ3-NPFFFREKKCALL mutant (Figure 2A) (one-way ANOVA: $F_{1,\ 28} = 55.41$, $p = 0.036$; Supplemental Table S2, A and B). Furthermore, the PIP3 generation was equally attenuated in cells expressing these two mutants compared with the WT-Gγ3–expressing cells (at $p = 0.05$) upon blue opsin activation (Figure 2B). These observations suggest that the hydrophobic character in the pre-CaaX region and its location relative to prenylated-*cys* regulate Gβγ signaling at the PM.

The effect of the last Gβ-interacting phe in Gγ on Gβγ signaling at the PM is minor. Because this conserved *phe* residue (*phe*65 in Gγ3) interacts with a hydrophobic pocket in Gβ (Akgoz *et al.*, 2002), we examined how vital its contribution is to the PM affinity and effector activation ability of Gβγ at the PM. Relative to WT-Gγ3 cells, cells expressing a mutant Gγ3 in which *phe*65 was replaced with a *gly* (Gγ3-*phe*65→*gly*: NPGREKKFFCALL) showed a nearly twofold lower $t_{1/2}$ (200 ± 20 vs. 115 ± 18 s), indicating an enhanced rate of Gβγ translocation (Figure 2A and Table 1). The enhanced ability of Gβγ translocation in these Gγ3 mutant-expressing cells is further validated by the elevated extent of translocation compared with WT-Gγ3 cells (29.7 ± 3.7 vs. 21.3 ± 2.2 AFU) (Figure 2A and Table 2) (one-way ANOVA: $F_{1,\ 40} = 4.28$, $p = 0.04511$; Supplemental Table S2, A and B). The increased translocation rate of the mutant can be due to the loss of proper orientation of Gγ with Gβ in the Gβγ dimer. An in vitro assay showed an ~40% reduction in PLCβ2 activity upon a mutation of an equivalent *phe* in Gγ5 (*phe*59→A) (Akgoz *et al.*, 2002). Nevertheless, compared with WT-Gγ3, Gγ3-*phe65*→*gly* mutant HeLa cells exhibited an ~40% reduction in the rate of PIP3 generation (4.0×10^{-3} s^{-1}) (one-way ANOVA: $F_{1,\ 54} = 15.66$, $p = 2.23 \times 10^{-4}$; Supplemental Table S3, A and B). In comparison to WT-Gγ3, this mutant Gγ3-expressing cell also exhibited a significantly reduced extent of PIP3 generation (76.6 ± 7.4 vs. 55.0 ± 6.2 AFU) (Figure 2B and Table 2) (one-way ANOVA: $F_{1,\ 77} = 4.39$, $p = 0.039$; Supplemental Table S4, A and B).

The contribution of positively charged residues in the pre-CaaX of Gγ to the PM affinity and signaling of Gβγ at the PM is minor. Both Gγ3 and Gγ9 have homologous regions at the beginning of pre-CaaX consisting of three residues, arg-glu-lys in Gγ3 and lys-glu-lys in Gγ9 (Figure 1A). We hypothesized that the positive charges of arg and lys side chains collectively allow Gβγ to transiently interact with the negatively charged polar head groups of PM phospholipids. In contrast, negatively charged glu may likely create a repulsive force (Figure 1C). Considering these opposite charge characteristics, "+ - +", we anticipated a "pseudo-spring"–like behavior allowing for transient interactions–repulsions for Gβγ with and from the PM (Figure 1C). We mutated these charged residues in the pre-CaaX regions of Gγ3 and Gγ9 to examine this hypothesis. We first generated a Gγ9 mutant of which lys-glu-lys residues in the pre-CaaX were replaced with three gly residues (Gγ9-lys-glu-lys→gly-gly-gly: NPFGGGGGCLIS). Cells expressing this Gγ9 mutant showed near-similar translocation ($t_{1/2} = 13 \pm 2$ s vs. 12 ± 1 s) (Figure 3A and Table 1) and PIP3 generation characteristics (rate = 2.6×10^{-3} s^{-1} vs. 2.1×10^{-3} s^{-1}) (Figure 3B and Table 2) to WT-Gγ9 cells (Table 1). Additionally, the extents of Gβγ translocation

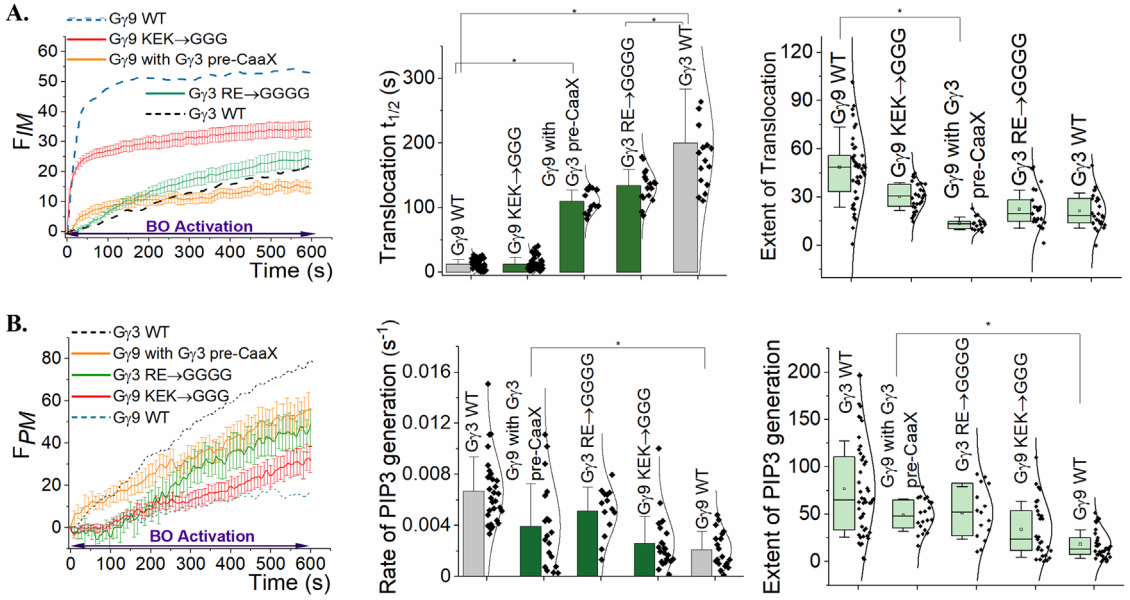

FIGURE 3: The effect of positively charged residues in the pre-CaaX on PM affinity and PI3K activation ability of Gβγ. (A) The plot shows Gi-coupled blue opsin activation-induced Gβγ translocation kinetics in HeLa cells expressing pre-CaaX region–mutated Gγ3 or Gγ9, to remove positively charged residues (F_{IM}, IM fluorescence). Average curves plotted using $n \geq 10$ cells from ≥3 independent experiments. Error bars: SEM. Differences in translocation $t_{1/2}$ and extent of translocation are shown, respectively, in the bar graph and whisker box plot. Error bars: SD. (B) The plot shows the influence of the above Gγ3 and Gγ9 mutants on PIP3 generation compared with WT-Gγ3 and Gγ9-expressing cells, upon blue opsin activation (F_{PM}, PM fluorescence). Average curves plotted using $n \geq 10$ cells from ≥3 independent experiments. Error bars: SEM. Bar graph compares rates of PIP3 generation while the whisker box plot shows the magnitude differences in PIP3 generation. Error bars: SD; *$p < 0.05$.

in cells expressing this Gγ9 mutant (as well as WT-Gγ9) and the Gγ3-phe-phe→gly-gly mutant were not significantly different (one-way ANOVA; $F_{1, 36} = 4.67$, $p = 0.04$) (Figure 3A; Supplemental Table S2, A and B). This further suggests the crucial contribution of the *phe-duo* for Gγ-PM interactions.

Because the mutant Gγ9-*lys-glu-lys→gly-gly-gly* (NPFGGG-GGCLIS) did not show a significant change in Gβγ activity at the PM compared with WT-Gγ9 cells, to further examine whether the "pseudo-spring" behavior exists, we generated a Gγ3 mutant by replacing *arg-glu* with two *gly* and also introducing two extra *gly* residues (Gγ3-*arg-glu→gly-gly-gly*-gly: NPFGGGGKKFFCALL). Interestingly, Gγ3-*arg-glu→gly-gly-gly*-gly mutant cells exhibited a minor reduction in PM affinity (Gβγ translocation $t_{1/2}$ = 134 ± 6 s) (Figure 3A and Table 1). However, the change in the rate of PIP3 generation in the mutant cells compared with WT-Gγ3 cells was not statistically significant (Figure 3B and Table 1). Overall, these data suggest that, unlike polybasic C-termini of Ras family proteins, contributions from the charged residues in the pre-CaaX of Gγ to the PM affinity and the PI3K activation ability of Gβγ are relatively minor.

Cells expressing a Gγ9 mutant carrying the entire pre-CaaX region of Gγ3 (Gγ9 with Gγ3 pre-CaaX: NPF**REKKFF**CLIS) showed an approximately ninefold slower translocation ($t_{1/2}$ = 110 ± 5 s) compared with WT-Gγ9–expressing cells ($t_{1/2}$ = 12 ± 1 s) (Figure 3A and Table 1). A one-way ANOVA ($F_{1, 59} = 30.78$, $p = 7.43 \times 10^{-7}$) showed that the extent of Gβγ translocation in these mutant Gγ9 cells is significantly lower than that of WT-Gγ9 cells. Compared with WT-Gγ9 cells, mutant Gγ9 cells also exhibited an approximately twofold higher rate of PIP3 generation (2.1×10^{-3} s^{-1} vs. 3.9×10^{-3} s^{-1}) (Figure 3B and Table 2). These data further validate our hypothesis that the pre-CaaX amino acids of Gγ tune the PM affinity and effector activation ability of Gβγ. Moreover, our findings emphasize the critical role of *phe-duo* adjacent to prenylated-*cys* in Gγ2, γ3, and Gγ4 in enhancing their PM affinity compared with the contribution from other residues in the pre-CaaX region.

Hydrophobic pre-CaaX residues in Gγ tune Gβγ-mediated partial adaptation of PIP2 hydrolysis

Gq-coupled GPCRs such as M1 and M3 muscarinic and gastrin releasing peptide (GRP) receptors efficiently induce the hydrolysis of phosphatidylinositol 4,5-bisphosphate (PIP2) into diacylglycerol (DAG) and inositol trisphosphate (IP3) via the activation of phospholipase-C β (PLCβ). However, within ~30–45 s after the initial Gq-GPCR activation, a universal partial adaptation of PIP2 hydrolysis begins, allowing for a partial synthesis of PIP2 at the PM (Figure 4A, up to 600 s). This adaptation should create low-intensity steady-state signaling of IP3 and DAG, where the equilibrium of PIP2 hydrolysis ⇋ synthesis is reached. Our recent work shows that this partial adaptation of PIP2 hydrolysis is governed by Gβγ (Weiland, 1978). Our data suggest that immediately upon Gq pathway activation, a highly potent $G\alpha q_{GTP}$-PLCβ-Gβγ sandwich complex is formed, which is responsible for the intense and near-complete PIP2 hydrolysis (Figure 4A, yellow box). Thus far, we have shown that Gβγ transiently interacts with the PM and control effectors in the vicinity, including PI3Ks and G protein–coupled inwardly rectifying potassium (GIRK) channels (Senarath *et al.*, 2018). Therefore, PM affinity-governed gradual dissociation of Gβγ from the PLCβ sandwich complex can be expected. This can generate the less-potent lipase $G\alpha q_{GTP}$-PLCβ, shifting the PIP2 hydrolysis ⇋ synthesis equilibrium to the right and reaching the steady-state. We further show that the kinetics of this PIP2 hydrolysis adaptation process and the steady-state intensity are Gγ-type dependent (Weiland, 1978). Because hydrophobic pre-CaaX residues of Gγ control the PM affinity of Gβγ (Figures 1 and 2), we examined whether the regulation of Gq-induced PIP2 hydrolysis adaptation is also pre-CaaX dependent.

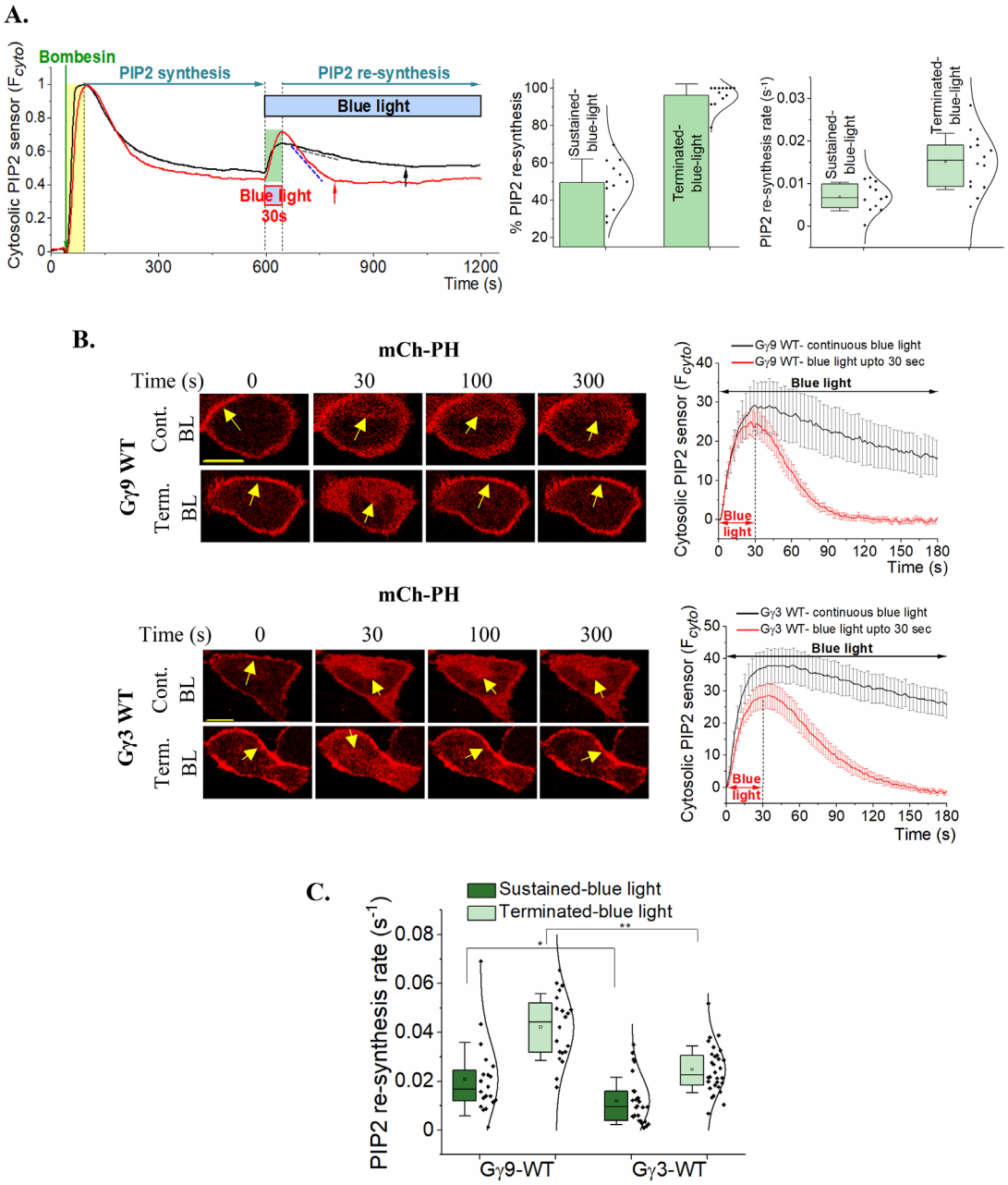

FIGURE 4: Gγ tunes Gβγ-mediated partial adaptation of PIP2 hydrolysis. (A) Plots of GRPR (Gq-GPCR)-induced PIP2 hydrolysis upon its activation with 1 μM bombesin, its partial adaptation, followed by Gβγ-mediated PIP2 rehydrolysis upon blue opsin (Gi-GPCR) activation (with blue light) and the second adaptation (PIP2 resynthesis). Red curve: fast (indicated by the blue tangent line) and complete adaptation of PIP2 upon termination of blue light after 30 s. Black curve: slower (indicated by the gray tangent line) and minor adaptation of PIP2 hydrolysis under sustained blue light. Both the red and black arrows show the steady-state PIP2 hydrolysis. Bar chart and whisker box plot show significantly lower PIP2 resynthesis (adaptation) with a slower rate under sustained blue opsin activation over near-complete and faster adaptation after blue light termination at 30 s. Error bar: SD. (B) Optogenetic signaling termination shows distinct regulation of Gαq-PLCβ–mediated PIP2 hydrolysis by Gγ9 and Gγ3. Time-lapse images of HeLa cells expressing GRPR, mCh-PH (PIP2 sensor), blue opsin, and GFP-Gγ9 (top two panels) or Gγ3 (bottom two panels) showing PIP2 hydrolysis and attenuation upon blue opsin activation in the Gq-active background (with GRPR activation). Images and corresponding plots show significantly different rates of PIP2 hydrolysis attenuation after termination of blue opsin activation at 30 s (red curves), which removes Gβγ rapidly, compared with the hydrolysis partial adaptation observed under continuous blue light (black curves). Yellow arrows indicate the PIP2 sensor (mCh-PH) initial localization on the PM, its movement to the cytosol (PIP2 hydrolysis), and partial relocalization to the PM (adaptation) during and after blue opsin activation. Average curves were plotted using $n \geq 10$ cells from ≥3 independent experiments. Scale bar: 5 μm. Error bars: SEM. (C) Whisker box plot shows the distinct regulation of PIP2 resynthesis rates due to its hydrolysis attenuation by Gγ3 and Gγ9 after termination of blue opsin activation at 30 s. Here, Gγ9-expressing cells showed a twofold higher attenuation rate compared with Gγ3-cells ($p < 0.01$). Under sustained blue opsin activation condition also Gγ9-expressing cells showed a twofold higher rate of PIP2 hydrolysis adaptation compared with Gγ3-expressing cells ($p < 0.05$). Error bars: SD; *$p < 0.05$, **$p < 0.01$.

Gγ type	$t_{1/2}$ (s)	Rate of PIP2 resynthesis (10^{-2} s^{-1})	
		Sustained blue light	Terminated blue light
Gγ3 WT	200.42 ± 20.20	1.2 ± 0.9	2.5 ± 1.0
Gγ3-FF→GG	93.28 ± 4.90	1.8 ± 0.8	3.4 ± 0.2
Gγ9 WT	12.15 ± 1.19	2.1 ± 0.2	4.2 ± 0.1
Gγ9-GG→FF	170.99 ± 11.74	1.6 ± 0.1	2.5 ± 0.6
Gγ9 with Gγ3 pre-CaaX	109.78 ± 4.67	1.3 ± 0.7	3.0 ± 0.5

TABLE 3: PIP2 resynthesis properties of Gγ mutants.

Gβγ modulates the partial adaptation of PIP2 hydrolysis. Gq-coupled GRPR, blue opsin, and the PIP2 sensor mCh-PH were expressed in HeLa cells. We employed blue opsin to gain precise temporal control of Gi/o heterotrimer activation and Gβγ generation (Figure 1D) (Senarath *et al.*, 2018). Before imaging, cells were incubated with 10 μM *11-cis*-retinal for 3 min in the dark, allowing for light-activatable blue opsin generation. Upon activation of GRPR with 1 μM bombesin, the characteristic transient PIP2 hydrolysis and its partial adaptation were observed (Figure 4A, up to 600 s). After the steady-state of PIP2 hydrolysis ⇋ synthesis is reached, we activated blue opsin by exposing cells to 445 nm blue light (1 Hz). In this Gαq-active background, Gi/o activation-induced Gβγ generation prompted rehydrolysis of PIP2 (Figure 4A, after 600 s, black trace under blue box). Here, we optogenetically controlled Gβγ availability under two blue light exposure conditions, that is, 1) blue light termination at the peak of PIP2 rehydrolysis (at ~30 s) (Figure 4A, red curve), and 2) continuous blue light (Figure 4A, black curve) (Table 3). In condition 1, blue opsin becomes inactive after ~50 ms of blue light termination (at 30 s) and $G\alpha i/o_{GTP} \rightarrow G\alpha i/o_{GDP}$ conversion occurs in ~100–400 ms (Tsang *et al.*, 2006; Sprang, 2016). Because Gi/o_{GDP} has greater than 100-fold higher affinity for Gβγ than that of $G\alpha i/o_{GTP}$ (Tuteja, 2009; Mahoney and Sunahara, 2016), an abrupt loss of Gβγ from the $G\alpha q_{GTP}$-PLCβ-Gβγ sandwich complex is expected. As anticipated, the termination of 30 s blue light illumination resulted in a faster PIP2 resynthesis (Figure 4A, red curve, blue tangent) compared with that in continuous blue light exposure (condition 2) (Figure 4A, black curve, gray tangent). The faster rate of PIP2 resynthesis under blue light termination resulted in the process reaching the steady-state within ~150 s (Figure 4A, red arrow). However, under continuous blue light exposure, it took more than ~6 min to reach the steady-state (Figure 4A, black arrow). The rate of PIP2 resynthesis after blue light termination was approximately twofold higher (7.0×10^{-3} s^{-1}) compared with that under sustained blue light (1.5×10^{-2} s^{-1}) (one-way ANOVA: $F_{1, 24} = 14.10$, $p = 7.26 \times 10^{-4}$) (Figure 4A, bar graph Supplemental Table S5). Furthermore, blue light termination resulted in a near-complete PIP2 resynthesis (96.2 ± 6.1%). In contrast, the continuous blue light exposure condition showed only a partial adaptation, with a relatively lower PIP2 resynthesis (49.4 ± 12.7%) (Figure 4A, box plot). We hypothesize that the distinct rates and extents of PIP2 resynthesis observed in the above two conditions result from the differences in Gβγ availability. Owing to $G\alpha i/o_{GTP}$ hydrolysis-associated abrupt removal of Gβγ upon blue light termination, $G\alpha q_{GTP}$-PLCβ-Gβγ is expected to experience a faster loss of Gβγ compared with the gradual loss of Gβγ under sustained blue light.

To further show Gβγ modulation of this Gi/o-governed PIP2 rehydrolysis ⇋ resynthesis response, we conducted similar experiments in cells additionally expressing either WT-Gγ9 or WT-Gγ3 (Figure 4A). After the partial adaptation of Gq-mediated PIP2 hydrolysis, we exposed cells to either 30 s or continuous blue light. Regardless of the Gγ type (whether Gγ9, Gγ3, or endogenous) compared with the continuous blue light condition, faster and near-complete PIP2 resynthesis responses were observed after blue light termination at 30 s (Figure 4, B and C). One-way ANOVA ($F_{1, 38} = 21.91$, $p = 3.57 \times 10^{-5}$) and Tukey post hoc tests showed a significantly higher mean rate (approximately twofold) of PIP2 resynthesis upon blue light termination compared with the sustained blue light condition. Under the above light conditions, HeLa cells expressing pre-CaaX mutants of Gγ9 and Gγ3 also exhibited similar and significant differences in the rates of PIP2 resynthesis (Supplemental Figure S4). Collectively, these data indicate that Gβγ availability is crucial for the efficacy of the Gq-governed lipase activity of PLCβ.

Hydrophobic pre-CaaX residues influence Gβγ-governed partial adaptation of PIP2 hydrolysis. These experiments were performed in cells that reached steady-state PIP2 hydrolysis after Gq-GPCR activation (like in Figure 4A, ~600 s). To examine how the type of Gγ modulates PIP2 adaptation in cells after its hydrolysis by Gi/o-GPCR activation, we activated blue opsin only for 30 s in HeLa cells also expressing mCh-PH and either Gγ3 or Gγ9. Upon termination of blue light at 30 s, WT-Gγ9 cells (Figure 5, blue trace) showed a twofold higher rate of hydrolysis adaptation (4.2×10^{-2} s^{-1}) compared with that of WT-Gγ3 cells (2.5×10^{-2} s^{-1}) (Figure 5, black trace). A Tukey post hoc test associated with a one-way ANOVA ($F_{1, 48} = 27.84$, $p = 3.12 \times 10^{-6}$) revealed that these mean rate differences are significant. Upon termination of blue opsin activation, a faster generation of $G\alpha i/o_{GDP}$ is likely to sequester Gβγ. The relative mobility of Gβγ, governed by its PM affinity, could dictate how fast Gβγ is removed from effectors. Therefore, we propose that the removal of Gβγ from the $G\alpha q_{GTP}$-PLCβ-Gβγ complex in the Gi/o-active background is determined by the PM affinity of Gβγ. Therefore, the higher rate of PIP2 hydrolysis adaptation in Gγ9-expressing cells can be understood by the low PM affinity of Gβγ9 (Ajith Karunarathne *et al.*, 2012) and the relatively transient PLCβ-Gβγ9 interactions. On the contrary, we anticipate Gβγ3 to have relatively robust interactions with PLCβ, allowing for a weaker PIP2 hydrolysis adaptation.

We next examined whether pre-CaaX residues influence the Gq-mediated lipase activity of the $G\alpha q_{GTP}$-PLCβ-Gβγ complex. As indicated by one-way ANOVA ($F_{1, 49} = 37.41$, $p = 2.34 \times 10^{-7}$) and Tukey post hoc tests, the rate of PIP2 hydrolysis adaptation was significantly lower in Gγ9-*gly-gly→phe-phe* mutant cells compared with that of WT-Gγ9 cells (Figure 5A, red trace and whisker box plot) (2.5×10^{-2} s^{-1} vs. 4.2×10^{-2} s^{-1}). Similarly, compared with WT-Gγ9 cells, cells with the Gγ9 mutant carrying the pre-CaaX of Gγ3 showed a significant reduction in PIP2 hydrolysis adaptation rate (4.2×10^{-2} s^{-1} vs. 3.0×10^{-2} s^{-1}; Figure 5A, orange trace and whisker box plot) (one-way ANOVA: $F_{1, 32} = 10.66$, $p = 0.00261$). These rate differences (Table 3) indicate that the introduction of a more hydrophobic character to the pre-CaaX of Gγ enhances the ability of Gβγ to

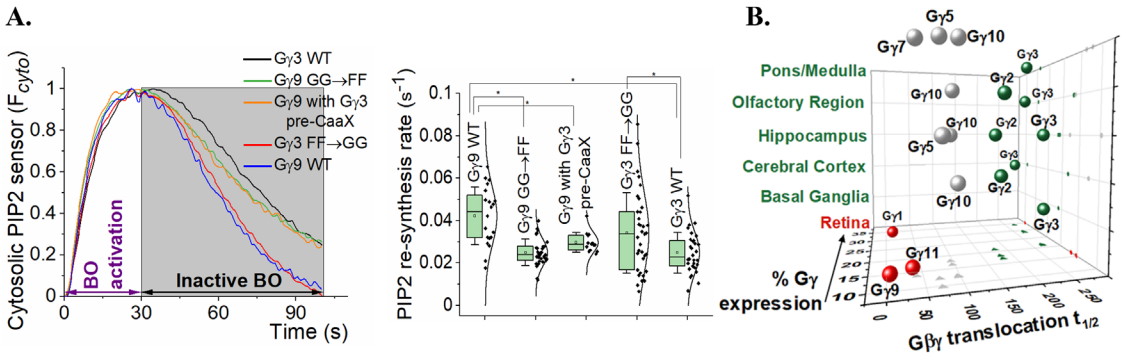

FIGURE 5: Pre-CaaX residues influence the rate of PIP2 hydrolysis termination. Cells expressing GRPR, mCh-PH, blue opsin, and either GFP-Gγ9, Gγ3, or their pre-CaaX mutants were first activated with 1 μM bombesin, allowing PIP2 hydrolysis and partial adaption to occur before the experiment. (A) The plot compares the dynamics of blue opsin–induced PIP2 hydrolysis (BO activation) up to 30 s and resynthesis after blue light termination in the Gq-active background. The whisker box plot shows that replacement (in Gγ3) or introduction (in Gγ9) of *phe-duo* next to the prenylated *cys* significantly alters the rates of PIP2 resynthesis compared with the corresponding Gγ WT. Average curves were plotted using $n \geq 10$ cells from ≥3 independent experiments. Error bars: SD. (B) Tissue-specific segregated mRNA expression of fast and slow translocating Gγ types. Human retina shows exclusive expression of fast translocating Gγ1, Gγ9, and Gγ11 (red). Note that these Gγs are excluded from the brain tissues. Brain tissues show predominant expression of Gγ2, Gγ3, and Gγ4 (*phe-duo* containing) (green) compared with other Gγs. Interestingly, fast translocating Gγs do not show a detectable expression in brain tissues. Gγs with relative expression above 10% were considered. Figures S5 and S6 shows Gγ diversity in cells within tissues. $^*p < 0.05$.

stimulate Gq-PLCβ signaling. Distinct Gβγ translocation profiles (Figure 1D) and PIP3 generation data (Figure 1E) show the reduction in the PM affinity of Gβγ in Gγ3-*phe-phe→gly-gly* mutant cells compared with that of WT-Gγ3 cells. As anticipated, a significantly higher rate of PIP2 hydrolysis adaptation was observed in the mutant Gγ3-*phe-phe→gly-gly* cells compared with WT-Gγ3 cells (3.4×10^{-2} s^{-1} vs. 2.5×10^{-2} s^{-1}) (Figure 5A) (one-way ANOVA: $F_{1,\ 63} = 5.92$, $p = 0.02$). Gβγ translocation is a direct indicator of the PM affinity of Gβγ. (Senarath *et al.*, 2016) Therefore, it likely captures even minor changes in the PM affinity of Gβγ. Though we observed significant changes in the PLCβ-governed PIP2 dynamics upon expression of Gγ mutants (relative to Gγ-WT) compared with Gβγ translocation, the sensitivity of the PIP2 hydrolysis-adaptation process to the changes in Gβγ PM affinity is reduced. This is not surprising because PIP2 hydrolysis and its adaptation upon PLCβ activation is one of the downstream processes regulated by Gβγ. Further, PIP2 and PLCβ are also controlled by regulators, including phosphatases, kinases, and calcium (Weiland, 1978). Therefore, it is not surprising to observe larger PLCβ activity changes only upon drastic changes to PM affinity and thus the availability of Gβγ at the PM.

The data of Gγ expression at the transcript level in different human tissues extracted from the FANTOM5 repository in the human protein atlas database show the tissue-specific expression of different Gγs in the human body (Uhlén *et al.*, 2015, 2017; Thul *et al.*, 2017). Here, we selected brain-associated 6 tissue types as a sample to illustrate the Gγ diversity. These transcriptomic data show that many distinct neurological centers of the brain, including the cerebral cortex, olfactory regions, and basal ganglia, express Gγ types such as Gγ2, γ3, and γ4 that contain *phe-duo* next to prenylated-*cys* (Figure 5B) (Uhlén *et al.*, 2015). Retina is an outlier, and unlike the brain regions, it does not express high PM affinity Gγ2, γ3, or γ4. It does not express even Gγ types with moderate-PM affinities (Figure 5B). Because the expressions were determined using complex tissue homogenates, the cell-type–specific Gγ diversity is not visible. However, distinct cell types have exhibited significant variability in Gγ expression in tissues at the protein level (Supplemental Figures S5 and S6). For instance, while bipolar cells show a prominent Gγ13 expression, Gγ1 and Gγ9 are the primary Gγs in rod and cone photoreceptor cells in the retina. In addition to its elevated expression in the ovary and prostate, Gγ3 protein has exhibited prominent expression in the cerebral cortex, corroborating with the transcriptomic data in Figure 5B (Sjöstedt *et al.*, 2018). Several other investigations also have indicated the unique expression profiles of Gγ types in different cell and tissue types (Fagerberg *et al.*, 2014; Gremel *et al.*, 2015; Syrovatkina *et al.*, 2016). Collectively considering our data and unique Gγ expression profiles in functionally specialized tissues and cells, including the retina and the brain, we propose that pre-CaaX residues in Gγ likely play a broader regulatory role in GPCR-G protein signaling.

DISCUSSION

We believe that the following remaining questions about Gβγ are crucial to have a deeper understanding of GPCR-G protein signaling: 1) Why do not all Gγ types promote Gβγ to activate effectors to a similar extent? 2) Why does Gγ show cell-tissue–specific expressions? 3) Could the relative orientation of Gβγ with the PM be important for Gβγ-effector interactions? 4) What makes Gγ2, γ3, and γ4 more efficient in regulating PM-bound Gβγ effectors? 5) Is sampling the PM for effectors by Gβγ governed by the CT of Gγ? Identification of the unique sequence properties of Gγ2-4 compared with the rest of the Gγ-pool, especially their *phe-duo* next to the prenylated-*cys* as a key regulator of Gβγ signaling at the PM, now allows us to answer the above questions and more. Compared with Gγ2–4, the rest of the geranylgeranylated Gγ types such as Gγ5, γ7, γ10, and γ12 that are lacking hydrophobic residues exhibited a significantly reduced Gβγ signaling at the PM (Senarath *et al.*, 2018). Therefore, we hypothesized that this *phe-duo* is an essential requirement in Gγ to display high Gβγ-effector activity at the PM. The perturbation of these residues in the current study revealed intricate molecular details of pre-CaaX residues and their relative location in the Gγ-CT in Gβγ signaling regulation.

The observed significant attenuation of Gβγ signaling after shifting *phe-duo* away from the prenylated-*cys* indicates that being

located away from the prenyl anchor and thus the reduced proximity of benzyl side chains in the shifted *phe-duo* to the PM likely reduces the PM affinity of Gβγ. When the *phe-duo* is next to the prenylated-*cys*, the prenyl anchor is likely to pull Gγ toward the PM, facilitating benzyl groups of *phe* to form strong hydrophobic interactions with the PM. This reinforcement appears to be an essential criterion in the pre-CaaX of Gγ to enhance the PM affinity and the effector interaction ability of Gβγ at the PM. This crucial involvement of the *phe-duo* was further confirmed by the reduced Gβγ signaling observed in Gγ mutant cells with *gly* or Gγ types lacking *phe* residues next to prenylated-*cys* (as in Gγ9). Data also indicate a moderate enforcement of Gβγ–PM interactions by other hydrophobic residues in the pre-CaaX, likely through hydrophobic interactions with the PM. For instance, compared with Gγ9, *leu* in Gγ1 pre-CaaX appears to provide a slightly higher PM affinity. Additionally, our data also indicate a lesser influence from the charged residues in the pre-CaaX, including *lys*, *arg*, and *glu*, on Gβγ signaling at the PM. This is a significant difference from prenylated Ras family proteins that primarily use poly-*lys* and thereby electrostatic interactions to enforce PM interactions.

Our data indicate that the influence of the Gγ prenylation type on the PM affinity and the signaling of Gβγ at the PM is not as strong as initially predicted. For instance, cells expressing predictably a farnesylated Gγ9 mutant with Gγ3 pre-CaaX exhibited a Gβγ-induced PIP3 generation resembling that of Gγ3 cells. We show that the type of prenylation in pre-CaaX mutated Gγs is intact and in agreement with its CaaX sequence (Supplemental Figure S2). Both the Gγ-WT and its pre-CaaX region–altered Gγ mutants showed similar sensitivity to their corresponding prenyltransferase inhibitors but not to the other kind. For instance, Gγ9-WT (pre-CaaX→NPFKEKGG) is farnesylated, and this farnesylation was inhibited by the farnesyltransferase inhibitor, Tipifranib, but not by the geranylgeranyltransferase inhibitor, GGTI286. Prenylation of its pre-CaaX mutant, Gγ9-*gly-gly→phe-phe* (pre-CaaX→NPFKEKFF), was also similarly inhibited by Tipifarnib, indicating that the mutagenesis of the pre-CaaX region does not alter the type of prenylation (Supplemental Figure S2). Our findings thus collectively suggest that the sequence properties of the pre-CaaX region of Gγ allow cells to have a broad range of Gβγ activities at the PM from "on" to "off" paradigms. These data also suggest that Gγ types are evolved to have relatively short PM-interacting pre-CaaX regions compared with other prenylated proteins (i.e., Ras family proteins). By installing or avoiding hydrophobic residues at specific locations in the pre-CaaX, Gγ types provide a range of PM affinities and effector activation abilities for Gβγ at the PM. The capacity of pre-CaaX residues to significantly modify Gq pathway-mediated PLCβ signaling further establishes the broader physiological relevance of the pre-CaaX region of Gγ. It also rationalizes the evolutionary significance of the existence of 12 Gγ types with distinct PM affinities. Is Gβγ translocation due to deprenylation? Unlike palmitoylated Gα that shows a rapid turnover at the PM through depalmitoylation (Huang *et al.*, 1999; Wedegaertner, 2012), Gγ prenylation is an irreversible process (Palsuledesai and Distefano, 2015; Wang *et al.*, 2017). Prenylation requires –aaX residues of the CaaX motif to proceed. Upon prenylation, –aaX is cleaved by RCE1 (Ras-converting CaaX endopeptidase 1), followed by ICMT (isoprenyl carboxyl methyltransferase)-induced carboxymethylation of prenylated-*cys* (Wright and Philips, 2006). Even if Gγ were to be deprenylated, reprenylation could not occur due to the permanent modification of the prenyltransferase-recognizing region of Gγ. Therefore Gβγ must be translocating with the prenylated Gγ.

The dominant expression of Gγ1, γ11, and γ9 as well as the exclusive absence of Gγ2, γ3, and γ4 in the retina photoreceptor cells (Figure 5B) can be understood by envisioning the possible consequences of their signaling outcomes. The observed slow adaptation of PIP2 hydrolysis in Gγ3 cells compared with Gγ9 cells indicates a slow termination of Gβγ3 effector signaling after termination of GPCR activity (Figure 5A). During vision transduction, upon the termination of opsin activation, $G\alpha_{transducin}$ and Gβγ should be reunited instantaneously, so that opsin can be ready for the next heterotrimer activation upon the photon reception. Therefore, we argue that the exclusion of Gγ2–4 and the inclusion of Gγ1, γ9, and γ11 in photoreceptor cells are essential for the acuity and brisk nature of phototransduction. In what way, then, does Gγ1, γ9, and γ11 facilitate vision signaling? Upon activation of opsin, Gβγ9 has shown a detectable translocation in <500 ms (Senarath *et al.*, 2016). Therefore, we propose that this rapid translocation allows for a complete and fast separation of $G\alpha_{transducin}$ from Gβγ, facilitating $G\alpha_{transducin}$-directed vision signaling. Further, the removal of Gβγ from the PM could eliminate unnecessary PM Gβγ signaling. The fast translocation of Gβγ may also be necessary to regenerate $G\alpha_{transducin}$ heterotrimers upon $G\alpha_{GDP}$ formation, allowing for signaling continuation. Though they show elevated expression in specific brain regions, the functional role/s of this exclusive expression of Gγ2, γ3, and γ4 are entirely unknown (Morishita *et al.*, 1997). This complexity is exacerbated by the fact that the majority of organs express Gγ types with moderate-PM affinities. Though they are geranylgeranylated, these Gγ types lack the *phe-duo* next to the prenylated-*cys*. This deficiency appears to provide the Gγs moderate-PM affinities between Gγ2–4 and Gγ1, γ9, and γ11. We, therefore, propose that, by having Gγ types with moderate-PM affinities, cells in most organs, unlike the eye (and possibly the brain), utilize Gβγ to maintain moderate effector signaling at the PM and some signaling in cell-interior regions such as the Golgi and endoplasmic reticulum (ER). Further investigations are needed to confirm these assumptions.

Reports suggest that Gβγ controls signaling in internal compartments of cells such as the Golgi (Saini *et al.*, 2010; Hewavitharana and Wedegaertner, 2015), mitochondria (Hewavitharana and Wedegaertner, 2012; Ahmed and Angers, 2013), and the nucleus (Kino *et al.*, 2005; Hewavitharana and Wedegaertner, 2012). Because current findings indicate a higher concentration of Gβγ in IMs upon GPCR activation in cells primarily expressing low PM-affinity Gγ types, we expect these cells to have dominant Gα signaling at the PM and Gβγ signaling in IMs. Our findings may also indicate that the pre-CaaX region of Gγ and thereby the PM affinity of Gβγ influence 1) the efficacy of heterotrimer-GPCR interaction and 2) the rate of Gβγ activity cessation upon termination of GPCR activity, as well as 3) the rates of GPCR phosphorylation and desensitization. However, these hypotheses need investigation. Our findings, additionally enabled by optogenetic GPCR-G protein signaling control, help in understanding the complex regulation of GPCR-G protein signaling at various cellular compartments and how cells achieve desired signaling selectivity based on Gβγ–membrane interactions. This knowledge may open avenues for pharmacological intervention.

MATERIALS AND METHODS

Request a protocol through *Bio-protocol*.

Reagents

The reagents bombesin (Tocris Bioscience, Bristol, UK), 11-*cis* retinal (National Eye Institute, Bethesda, MD), and Tipifarnib and GGTI286 (Cayman Chemical, Ann Arbor, MI) were dissolved in appropriate solvents according to manufacturer's instructions and diluted in 1% Hanks' Balanced Salt solution (HBSS) supplemented with $NaHCO_3$ or regular cell culture medium before being added to cells.

DNA constructs and cell lines

For the engineering of DNA constructs used, mCh-PH has been described previously (Kankanamge *et al.*, 2019). GRPR was a kind gift from the lab of Zhou-Feng Chen at Washington University, St. Louis, MO. Blue opsin-mTurquoise, GFP-Gγ9, GFP-Gγ3, mCh-Gβ1, and Akt-PH-mCh were kindly provided by N. Gautam's lab, Washington University, St. Louis, MO. Gγ3 and Gγ9 mutants were generated by PCR amplifying the parent constructs in pcDNA3.1 (GFP-Gγ3 and GFP-Gγ9) with overhangs containing expected nucleotide mutations and *Dpn*I (NEB) digestion (to remove the parent construct) followed by Gibson assembly (NEB) (Ratnayake *et al.*, 2017). The HeLa cell line was originally purchased from the American Type Culture Collection (ATCC) and authenticated using a commercial kit to amplify nine unique STR loci.

Cell culture and transfections

HeLa cells used in Gβγ translocation, PIP3 generation, and PIP2 hydrolysis and adaptation experiments were cultured in MEM (from CellGro) supplemented with 10% heat-inactivated dialyzed fetal bovine serum (DFBS; from Atlanta Biologicals) and 1% penicillin–streptomycin (PS) in 60 mm tissue culture dishes and maintained in a 37°C, 5% CO_2 incubator. When the cells reach ~80% confluency, they are lifted from the dish using versene-EDTA (CellGro) and resuspended in their growth medium at a cell density of 1×10^6 /ml. For imaging experiments (translocation, PIP3 generation, and PIP2 hydrolysis), cells were seeded on 35 mm cell culture–grade glass-bottomed dishes (Cellvis) at a density of 8×10^4 cells. The day following cell seeding, cells were transfected with appropriate DNA combinations using Lipofectamine 2000 transfection reagent (Invitrogen) according to the manufacturer's protocol and stored in a 37°C, 5% CO_2 incubator. Cells were replenished with the growth medium after 5 h and were imaged after 16 h of transfection.

Live cell imaging to monitor Gβγ translocation, PIP3 generation, and PIP2 hydrolysis and subsequent synthesis

A spinning-disk XD confocal TIRF (total internal reflection) imaging system with a Nikon Ti-R/B inverted microscope, a Yokogawa CSU-X1 spinning disk unit (5000 rpm), an Andor FRAP-PA (fluorescence recovery after photobleaching and photoactivation) module, a laser combiner with 40–100 mW four solid-state lasers (with 445, 488, 515, and 594 nm wavelengths), and an iXon ULTRA 897BV back-illuminated deep-cooled EMCCD camera were used to capture time-lapse image series of live cells. In Gβγ translocation and PIP3 generation experiments, imaging was performed using a 60×, 1.4 NA (numerical aperture) oil objective. To examine the Gβγ translocation, GFP fluorescent tags on Gγ subunits (WTs and mutants) were imaged in every 1 s interval using 488 nm excitation–515 nm emission for 10 min. In PIP3 generation and PIP2 hydrolysis experiments, mCherry-tagged PIP3 and PIP2 sensors, Akt-PH and PH, were imaged using 594 nm excitation–630 nm emission red laser.

Quantification of Gβγ translocation, PIP3 generation, and PIP2 hydrolysis

Digital image analyses were performed using Andor iQ 3.1 software. In translocation and PIP2 experiments, the background-subtracted fluorescence intensity increase in IMs of individual cells was captured. Pre- and poststimulation images were generated by binning (×4) at the equilibrium. Initial baseline intensity values were subtracted from intensity values at regions of interest (ROIs) from multiple cells and single-cell fluorescence averages were plotted versus time to monitor the dynamics of translocation. The number of cells (usually one ROI per cell) and the number of independent experiments are provided in the figure legends. In PIP3 generation experiments, the background-subtracted PIP3 sensor (Akt-PH-mCh) fluorescence on the PM was captured and processed similar to Gγ translocation and PIP2 hydrolysis.

Statistical data analysis

Statistical analysis and data plotting were performed using OriginPro software (OriginLab Corporation). Results of all quantitative assays (Gβγ translocation, PIP3 generation, PIP2 hydrolysis) are expressed as mean ± SEM from *n* numbers of cells (indicated in the figure legends) from multiple independent experiments. After obtaining all of the baseline-subtracted data, PIP3 generation and PIP2 resynthesis rates were calculated using the Nonlinear Curve Fitting tool (NLFit) in OriginPro. In the NLFit tool, each plot was fitted to DoseResp (Dose-Response) function under the Pharmacology category by selecting the relevant range of data to be fitted. The mean values of hill slopes (P) obtained for each nonlinear curve fitting are presented as mean rates of PIP3 generation or PIP2 resynthesis. Similarly, employing the NLFit tool, Gβγ translocation plots were fitted to the MichaelisMenten function under the Pharmacology category to determine the $t_{1/2}$ of Gβγ translocation. The mean values of K_m obtained from nonlinear curve fitting for all cells are given as mean Gβγ translocation $t_{1/2}$. One-way ANOVA statistical tests were performed using OriginPro software to determine the statistical significance of mean signaling responses in different experiments. After inserting raw signaling response data from each cell for various experiments, the Tukey's mean comparison test was performed at the $p < 0.05$ significance level for the one-way ANOVA statistical test.

ACKNOWLEDGMENTS

We acknowledge N. Gautam, Washington University, St. Louis, MO, for providing us with plasmid DNA for GFP-GPI, G proteins (GFP-Gγ3 and Gγ9), and PIP3 sensor (Akt-PH-mCherry). We thank Diniti Welivita for the drawings in Figure 1C and Allison Boyer and Joanne Taylor for comments. We thank the National Eye Institute for 11-*cis*-retinal. We acknowledge The University of Toledo and the National Institutes of Health National Institute of General Medical Sciences (Grant number 1R15GM126455-01A1) for funding.

REFERENCES

Ahmed SM, Angers S (2013). Emerging non-canonical functions for heterotrimeric G proteins in cellular signaling. J Recept Signal Transduct Res 33, 177–183.

Ajith Karunarathne WK, O'Neill PR, Martinez-Espinosa PL, Kalyanaraman V, Gautam N (2012). All G protein βγ complexes are capable of translocation on receptor activation. Biochem Biophys Res Commun 421, 605–611.

Akgoz M, Azpiazu I, Kalyanaraman V, Gautam N (2002). Role of the G protein γ subunit in βγ complex modulation of phospholipase Cβ function. J Biol Chem 277, 19573–19578.

Anfinsen CB (1973). Principles that govern the folding of protein chains. Science 181, 223–230.

Czysz AH, Schappi JM, Rasenick MM (2015). Lateral diffusion of Gαs in the plasma membrane is decreased after chronic but not acute antidepressant treatment: role of lipid raft and non-raft membrane microdomains. Neuropsychopharmacology 40, 766–773.

Das BB, Park SH, Opella SJ (2015). Membrane protein structure from rotational diffusion. Biochim Biophys Acta 1848, 229–245.

Dowhan W (1997). Molecular basis for membrane phospholipid diversity: why are there so many lipids? Annu Rev Biochem 66, 199–232.

Engelman DM (2005). Membranes are more mosaic than fluid. Nature 438, 578–580.

Escriba PV, Sanchez-Dominguez JM, Alemany R, Perona JS, Ruiz-Gutierrez V (2003). Alteration of lipids, G proteins, and PKC in cell membranes of elderly hypertensives. Hypertension 41, 176–182.

Fagerberg L, Hallström BM, Oksvold P, Kampf C, Djureinovic D, Odeberg J, Habuka M, Tahmasebpoor S, Danielsson A, Edlund K, *et al*. (2014). Analysis of the human tissue-specific expression by genome-wide I\ integration of transcriptomics and antibody-based proteomics. Mol Cell Proteomics 13, 397–406.
Frick M, Schmidt K, Nichols BJ (2007). Modulation of lateral diffusion in the plasma membrane by protein density. Curr Biol 17, 462–467.
Gremel G, Wanders A, Cedernaes J, Fagerberg L, Hallstrom B, Edlund K, Sjostedt E, Uhlen M, Ponten F (2015). The human gastrointestinal tract-specific transcriptome and proteome as defined by RNA sequencing and antibody-based profiling. J Gastroenterol 50, 46–57.
Hepler JR (2014). G protein coupled receptor signaling complexes in live cells. Cell Logist 4, e29392.
Hessel E, Heck M, Muller P, Herrmann A, Hofmann KP (2003). Signal transduction in the visual cascade involves specific lipid-protein interactions. J Biol Chem 278, 22853–22860.
Hewavitharana T, Wedegaertner PB (2012). Non-canonical signaling and localizations of heterotrimeric G proteins. Cell Signal 24, 25–34.
Hewavitharana T, Wedegaertner PB (2015). PAQR3 regulates Golgi vesicle fission and transport via the Gβγ-PKD signaling pathway. Cell Signal 27, 2444–2451.
Higgins JB, Casey PJ (1996). The role of prenylation in G-protein assembly and function. Cell Signal 8, 433–437.
Huang C, Duncan JA, Gilman AG, Mumby SM (1999). Persistent membrane association of activated and depalmitoylated G protein α subunits. Proc Natl Acad Sci USA 96, 412–417.
Jastrzebska B, Debinski A, Filipek S, Palczewski K (2011). Role of membrane integrity on G protein-coupled receptors: rhodopsin stability and function. Prog Lipid Res 50, 267–277.
Kankanamge D, Tennakoon M, Weerasinghe A, Cedeno-Rosario L, Chadee DN, Karunarathne A (2019). G protein αq exerts expression level-dependent distinct signaling paradigms. Cell Signal 58, 34–43.
Khan MS, Dosoky NS, Williams JD (2013). Engineering lipid bilayer membranes for protein studies. Int J Mol Sci 14, 21561–21597.
Kino T, Kozasa T, Chrousos GP (2005). Statin-induced blockade of prenylation alters nucleocytoplasmic shuttling of GTP-binding proteins γ2 and β2 and enhances their suppressive effect on glucocorticoid receptor transcriptional activity. Eur J Clin Invest 35, 508–513.
Knight JD, Falke JJ (2009). Single-molecule fluorescence studies of a PH domain: new insights into the membrane docking reaction. Biophys J 96, 566–582.
Mahoney JP, Sunahara RK (2016). Mechanistic insights into GPCR-G protein interactions. Curr Opin Struct Biol 41, 247–254.
Matsuda T, Takao T, Shimonishi Y, Murata M, Asano T, Yoshizawa T, Fukada Y (1994). Characterization of interactions between transducin α/βγ-subunits and lipid-membranes. J Biol Chem 269, 30358–30363.
Maurer-Stroh S, Koranda M, Benetka W, Schneider G, Sirota FL, Eisenhaber F (2007). Towards complete sets of farnesylated and geranylgeranylated proteins. PLoS Comput Biol 3, e66.
Morishita R, Saga S, Kawamura N, Hashizume Y, Inagaki T, Kato K, Asano T (1997). Differential localization of the γ 3 and γ 12 subunits of G proteins in the mammalian brain. J Neurochem 68, 820–827.
Nishimura A, Kitano K, Takasaki J, Taniguchi M, Mizuno N, Tago K, Hakoshima T, Itoh H (2010). Structural basis for the specific inhibition of heterotrimeric Gq protein by a small molecule. Proc Natl Acad Sci USA 107, 13666–13671.
O'Neill PR, Karunarathne WK, Kalyanaraman V, Silvius JR, Gautam N (2012). G-protein signaling leverages subunit-dependent membrane affinity to differentially control βγ translocation to intracellular membranes. Proc Natl Acad Sci USA 109, E3568–E3577.
Owen DM, Williamson D, Rentero C, Gaus K (2009). Quantitative microscopy: protein dynamics and membrane organisation. Traffic 10, 962–971.
Palsuledesai CC, Distefano MD (2015). Protein prenylation: enzymes, therapeutics, and biotechnology applications. ACS Chem Biol 10, 51–62.
Pedone KH, Hepler JR (2007). The importance of N-terminal polycysteine and polybasic sequences for G14α and G16α palmitoylation, plasma membrane localization, and signaling function. J Biol Chem 282, 25199–25212.
Ramadurai S, Duurkens R, Krasnikov VV, Poolman B (2010). Lateral diffusion of membrane proteins: consequences of hydrophobic mismatch and lipid composition. Biophys J 99, 1482–1489.
Ratnayake K, Kankanamge D, Senarath K, Siripurapu P, Weis N, Tennakoon M, Payton JL, Karunarathne A (2017). Measurement of GPCR-G protein activity in living cells. Methods Cell Biol 142, 1–25.
Resh MD (2013). Covalent lipid modifications of proteins. Curr Biol 23, R431–R435.
Saini DK, Karunarathne WK, Angaswamy N, Saini D, Cho JH, Kalyanaraman V, Gautam N (2010). Regulation of Golgi structure and secretion by receptor-induced G protein βγ complex translocation. Proc Natl Acad Sci USA 107, 11417–11422.
Samaradivakara S, Kankanamge D, Senarath K, Ratnayake K, Karunarathne A (2018). G protein γ (Gγ) subtype dependent targeting of GRK2 to M3 receptor by Gβγ. Biochem Biophys Res Commun 503, 165–170.
Seabra MC (1998). Membrane association and targeting of prenylated Ras-like GTPases. Cell Signal 10, 167–172.
Senarath K, Payton JL, Kankanamge D, Siripurapu P, Tennakoon M, Karunarathne A (2018). Gγ identity dictates efficacy of Gβγ signaling and macrophage migration. J Biol Chem 293, 2974–2989.
Senarath K, Ratnayake K, Siripurapu P, Payton JL, Karunarathne A (2016). Reversible G protein βγ9 distribution-based assay reveals molecular underpinnings in subcellular, single-cell, and multicellular GPCR and G protein activity. Anal Chem 88, 11450–11459.
Simons K, Vaz WL (2004). Model systems, lipid rafts, and cell membranes. Annu Rev Biophys Biomol Struct 33, 269–295.
Singer SJ, Nicolson GL (1972). The fluid mosaic model of the structure of cell membranes. Science 175, 720–731.
Sjöstedt E, Sivertsson Å, Hikmet Noraddin F, Katona B, Näsström Å, Vuu J, Kesti D, Oksvold P, Edqvist P-H, Olsson I, *et al*. (2018). Integration of transcriptomics and antibody-based proteomics for exploration of proteins expressed in specialized tissues. J Proteome Res 17, 4127–4137.
Sprang SR (2016). Invited review: activation of G proteins by GTP and the mechanism of Gα-catalyzed GTP hydrolysis. Biopolymers 105, 449–462.
Syrovatkina V, Alegre KO, Dey R, Huang X-Y (2016). Regulation, signaling, and physiological functions of G-proteins. J Mol Biol 428, 3850–3868.
Tennakoon M, Senarath K, Kankanamge D, Ratnayake K, Wijayaratna D, Olupothage K, Ubeysinghe S, Martins-Cannavino K, Hébert TE, Karunarathne A (2021). Subtype-dependent regulation of Gβγ signalling. Cell Signal 82, 109947.
Tesmer VM, Kawano T, Shankaranarayanan A, Kozasa T, Tesmer JJ (2005). Snapshot of activated G proteins at the membrane: the Gαq-GRK2-Gβγ complex. Science 310, 1686–1690.
Thul PJ, Åkesson L, Wiking M, Mahdessian D, Geladaki A, Ait Blal H, Alm T, Asplund A, Björk L, Breckels LM, *et al*. (2017). A subcellular map of the human proteome. Science 356, eaal3321.
Tsang SH, Woodruff ML, Chen CK, Yamashita CY, Cilluffo MC, Rao AL, Farber DB, Fain GL (2006). GAP-independent termination of photoreceptor light response by excess γ subunit of the cGMP-phosphodiesterase. J Neurosci 26, 4472–4480.
Tuteja N (2009). Signaling through G protein coupled receptors. Plant Signal Behav 4, 942–947.
Uhlén M, Fagerberg L, Hallström BM, Lindskog C, Oksvold P, Mardinoglu A, Sivertsson Å, Kampf C, Sjöstedt E, Asplund A, *et al*. (2015). Proteomics. Tissue-based map of the human proteome. Science 347, 1260419.
Uhlén M, Zhang C, Lee S, Sjöstedt E, Fagerberg L, Bidkhori G, Benfeitas R, Arif M, Liu Z, Edfors F, *et al*. (2017). A pathology atlas of the human cancer transcriptome. Science 357, eaan2507.
Vogler O, Barcelo JM, Ribas C, Escriba PV (2008). Membrane interactions of G proteins and other related proteins. Biochim Biophys Acta 1778, 1640–1652.
Vogler O, Casas J, Capo D, Nagy T, Borchert G, Martorell G, Escriba PV (2004). The Gβγ dimer drives the interaction of heterotrimeric Gi proteins with nonlamellar membrane structures. J Biol Chem 279, 36540–36545.
Wang J, Yao X, Huang J (2017). New tricks for human farnesyltransferase inhibitor: cancer and beyond. MedChemComm 8, 841–854.
Wedegaertner PB (2012). G protein trafficking. Subcell Biochem 63, 193–223.
Wedegaertner PB, Wilson PT, Bourne HR (1995). Lipid modifications of trimeric G proteins. J Biol Chem 270, 503–506.
Weiland G (1978). [The enzyme-linked immunosorbent assay (ELISA)—a new serodiagnostic method for the detection of parasitic infections (author's transl)]. MMW Munch Med Wochenschr 120, 1457–1460.
Wennerberg K, Rossman KL, Der CJ (2005). The Ras superfamily at a glance. J Cell Sci 118, 843–846.
Wright LP, Philips MR (2006). Thematic review series: lipid posttranslational modifications. CAAX modification and membrane targeting of Ras. J Lipid Res 47, 883–891.